Preparation of Reduced Graphene Oxide/Ultrathin BiOCl Nanosheet Composites with Enhanced Electrochemical Behavior and Photocatalytic Performance

Wei Wang, Mingyi He[*], Huan Zhang, Yatang Dai[*]

School of Materials Science and Engineering, Southwest University of Science and Technology, Mianyang 621010, China
[*]E-mail: sialons@gmail.com, daiyt2003@163.com

In this study, uniform reduced graphene oxide (rGO)-ultrathin (U) BiOCl nanosheet composites were obtained via a facile hydrothermal method. The rGO-(U)BiOCl composites exhibited enhanced electrochemical behavior and photocatalytic activities for rhodamine B degradation, which was better than that of bare BiOCl with similar size. Moreover, the photodegradation efficiency for rGO(5 wt%)-(U)BiOCl was highest under UV light irradiation and visible light irradiation.

1. INTRODUCTION

Photocatalysis has received much attention in recent years because of its highly efficient, non-polluting, and energy-saving characteristics [1-3]. These characteristics allow the photocatalysts to convert hydrogen or solar light energy into chemical energy while degrading pollutants [4,5].

Many photocatalysts, such as TiO_2, ZnO, CdS, and ZrO_2, have the ability to degrade pollutants [6,7]. Among numerous photocatalysts, BiOCl has been extensively investigated because of its unique properties, including higher catalytic efficiency than many other photocatalysts [8]. However, the band gap (3.2–3.5 eV) of BiOCl limits its photocatalytic activity in decomposing organic pollutants.

Graphene is a 2D carbon-based nanomaterial with π-conjugation and single atomic thickness. More importantly, graphene is reported to have zero band gaps, leading to excellent mobility of charge carriers as photocatalyst. Given its unique electronic band structure, graphene can absorb solar energy from ultraviolet (UV) light to near-infrared light [9]. Moreover, graphene has been reported to be an

excellent electron acceptor because of its 2D π-conjugation structure [10]. Therefore, coupling BiOCl with graphene has been intensively studied to enhance the photocatalytic performance of UV light.

Gao et al. [11] obtained graphene/BiOCl (GR/BiOCl) nanocomposite photocatalysts via a facile chemical bath method, providing a very good reference to the fabrication of chemically bonded GR/semiconductor compounds and facilitating their applications in environmental protection, photo-electrochemical conversion, and photocatalytic decomposition of water. Yang et al. [12] prepared BiOCl-rGO composites with enhanced photocatalytic performance, which exhibited high photocatalytic activity for the photodegradation of methyl orange under visible light irradiation (lambda > 420 nm). Liu et al. [13] revealed the relationship between the electrochemical performance and photocatalytic activity of BiOCl in the degradation of organic pollutants. However, the photocatalytic performance of ultrathin BiOCl nanosheets and rGO nanocomposites is rarely studied.

In this paper, a facile and large-scale preparation method of rGO-(U)BiOCl photocatalysts was studied using a low-temperature hydrothermal technique at 90 °C. Rhodamine B (RhB) was used as the target degradation content to investigate the effects of graphene on the photocatalytic activity of BiOCl. Results showed that the obtained rGO-(U)BiOCl exhibited excellent electrochemical behavior and photocatalytic performance enhanced by graphene. In particular, the degradation time under visible light irradiation of rGO-(U)BiOCl photocatalysts was almost reduced to half compared with bare BiOCl nanosheets.

2. EXPERIMENTAL SECTION

2.1 Chemicals

Graphite (8000 mesh) was purchased from Aladdin Industrial Corporation. H_2SO_4 (98%), H_2O_2 (30%), ammonia (37%), $Bi(NO_3)_3.5H_2O$, HNO_3, potassium permanganate, hydrochloric acid (36%−38%), and RhB were obtained from Chengdu Kelong Chemical Corporation.

2.2 Preparation of Graphene Oxide (GO)

GO was prepared using a modified Hummers method as described in previous studies [14,15]. In a typical experiment, graphite and $KMnO_4$ were added to an ice bath with sulfuric acid. After continuous stirring for 2 h at 0 °C, the solution was added dropwise into water at a temperature below 98 °C. Subsequently, H_2O_2 was added into the solution. Finally, a bright yellow solution was obtained, filtered, and washed with 5% hydrochloric acid, ethanol, and distilled water at least three times.

2.3 Preparation of GO-BiOCl

The prepared GO was dissolved in water through sonication. About 30 mL of Bi(NO)3 (0.2 mol/L) and 1 mL of HCl (37 wt%) were added with vigorous stirring. Ammonia was added dropwise into the solution to adjust the pH to 10 when white products slowly appeared. The

ultrasonically prepared GO was slowly added to the solution, and the temperature was adjusted to 90 °C. Subsequently, 100 μL of hydrazine hydrate was added to the solution. After 2 h, we obtained a gray-colored product. After vacuum filtration, washing with distilled water, and drying at 60 °C, we obtained the final product.

2.4 Characterization

X-ray powder diffraction (XRD) analysis was carried out using PANalytical X'Pert PRO high-intensity Cu Ka ($\lambda = 1.5406$ Å). The field-emission SEM measurements were carried out using ZEISS Ultra 55, which was operated at the acceleration voltage of 15 kV. Raman spectra of the samples were performed using Micro-Raman Spectroscopy System (Renishaw InVia) at room temperature (RT). A continuous wave argon laser ($\lambda = 514$ nm) was used as excitation light source, and data collection ranged from 100 cm^{-1} to 3000 cm^{-1}. TG-DTA was carried out by SDT Q600 in air at a heating rate of 10 °C min^{-1} from 20 °C to 800 °C. UV–vis DRS were recorded on a UV–vis spectrometer (SDT Q600).

2.5 Electrochemical measurement

Electrochemical impedance spectroscopy (EIS) was measured on a IM 6 (Germany) electrochemical workstation with a standard three-electrode configuration. In this measurement, platinum plate was selected as counter electrode, Ag/AgCl was chosen as reference electrode. And the EIS test was carried out in Na$_2$SO$_4$ (0.5 mol/L) solution, which was performed at open circuit potential with 10 mV amplitude of the sinusoidal wave. The EIS test was carried out at room temperature.

## 2.6 Photocatalytic Activity Test

Photocatalytic reaction was carried out in a homemade photocatalytic reactor. Photocatalytic test was done through the catalytic degradation of RhB under UV light. The UV ($\lambda = 365$ nm) and visible light source was a Xe arc lamp, and 50 mL beakers served as catalytic vessels. In this experiment, 0.01 g of BiOCl sample was added into 100 mL of RhB solution (10 mg/L) at RT. The distance from the lamp to the RhB solution was 15 cm, and the length of the lamp was 10 cm. Prior to irradiation, the suspension was stirred in the dark to ensure the establishment of an adsorption-desorption equilibrium between the photocatalyst and RhB. After catalysis, the solution was subjected to high-speed centrifugation to remove the photocatalyst inside and obtain the upper clear liquid. The concentration of RhB was then analyzed using a Shimadzu UV2800 spectrophotometer. All measurements were carried out at RT.

3. RESULTS AND DISCUSSION
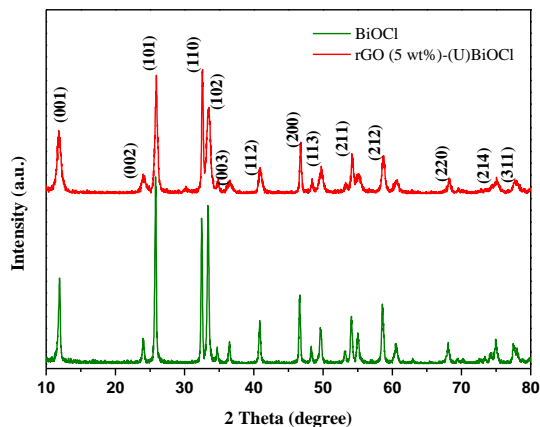
Figure 1. XRD patterns of the as-synthesized bare BiOCl and rGO(5 wt%)-(U)BiOCl.

Figure 1 shows the typical XRD patterns of the as-synthesized bare BiOCl ultrathin nanosheets and rGO(5 wt%)-(U)BiOCl nanocomposites. The diffraction peak positions of the prepared BiOCl were identical to the standard cards with tetragonal BiOCl (JCPDS no. 73-2060), which suggested that the prepared BiOCl had a monoclinic structure. Moreover, the rGO(5 wt%)-(U)BiOCl nanocomposite demonstrated very weak characteristic peaks of rGO probably because of its low content with lattice constants of a = b = 3.890 Å and c = 7.890 Å.
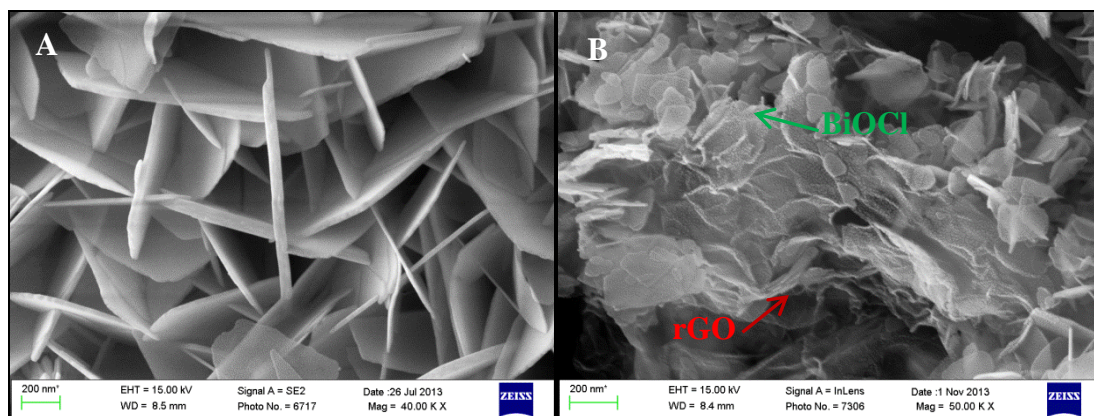
Figure 2. SEM images of synthesized BiOCl (a) and rGO-(U)BiOCl (b).

The morphologies and structures of the as-synthesized BiOCl and rGO-(U)BiOCl were characterized by SEM (Figure 2). The BiOCl monolithic length was 600–800 nm, and the width was about 20–60 nm. As illustrated in Figure 2, graphene films were observed on the surface of BiOCl, confirming the successful synthesis of rGO(5 wt%)-(U)BiOCl nanocomposites.
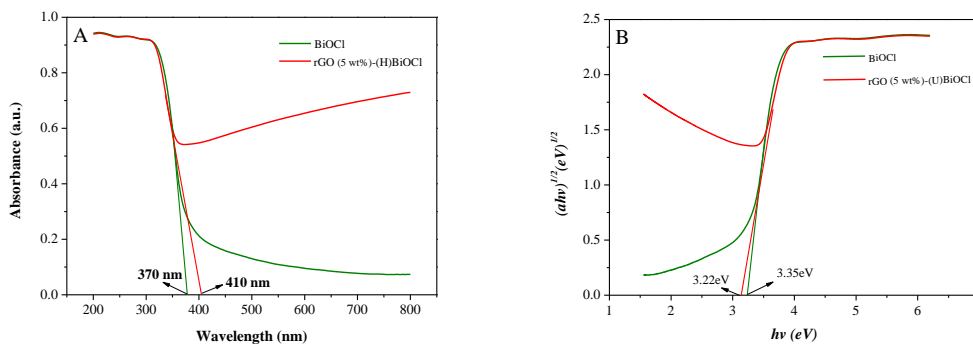
Figure 3. UV–vis diffuse reflectance spectra of different samples (A); plots of (ahv)1/2 versus photon energy (hv) for different samples (B).

Figure 3 shows the UV–vis diffuse reflectance spectra (DRS) and photon energies of BiOCl and rGO(5 wt%)-(U)BiOCl nanocomposites. The intense absorption edges of BiOCl and rGO(5 wt%)-(U)BiOCl were at 370 and 410 nm, respectively (Figure 3(A)).

As a crystalline semiconductor, the optical absorption near the band edge follows the formula: [16,17]

$$\alpha h v = A(h v - E_g)^{n/2}$$

where α, v, E_g, and A are the absorption coefficient, light frequency, band gap energy, and α constant, respectively; n depends on the characteristics of the transition in a semiconductor. For BiOCl, the value of n is estimated to be 4, which indicates the indirect transition of the BiOCl nanosheets.
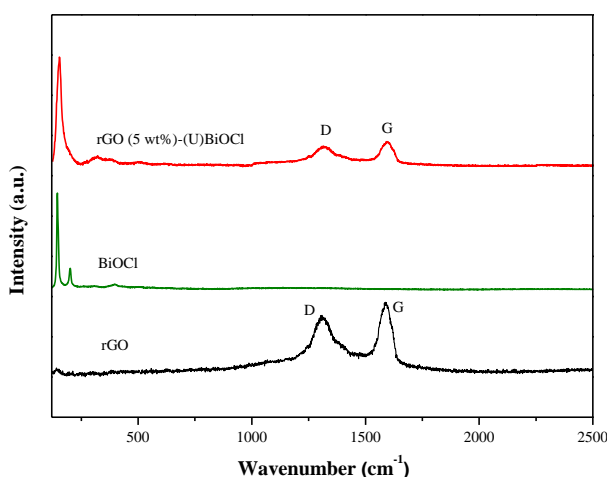

Figure 4. Raman spectra for rGO, BiOCl, and rGO-(U)BiOCl.

As illustrated in Figure 3(B), the band gaps of BiOCl and rGO(5 wt%)-(U)BiOCl were 3.35 and 3.22 eV, respectively. These results clearly demonstrated the band gap narrowing of the rGO-

BiOCl nanocomposites, which was probably carried out through the incorporation of intermediate energy levels into the band gap by BiOC bonds between BiOCl and rGO [18].

In Figure 3(A), we found that rGO-(U)BiOCl exhibited higher UV and visible light absorption than BiOCl. This phenomenon was caused by the ultra-high specific surface area of graphene, excellent mobility of charge carriers, and extremely high theoretical specific surface area [19, 20]. Therefore, the rGO-(U)BiOCl composites would be excellent photocatalysts under both UV and visible light.

To further examine the structural characterization of the products, Raman spectra measurement was performed. Figure 4 shows the Raman spectra of rGO, BiOCl, and rGO-(U)BiOCl. Two peaks at 1350 (D peaks) and 1580 cm^{-1} (G peaks) could be observed in the rGO Raman spectra, indicating the successful reduction of GO [21, 22]. BiOCl showed two characteristic peaks at 144 and 199 cm^{-1}. Most importantly, the characteristic peaks of the rGO-(U)BiOCl composites at 144, 1350, and 1580 cm^{-1} could be ascribed to the characteristic peak of BiOCl (144 cm^{-1}) and rGO (1350 and 1580 cm^{-1}). These results confirmed the successful preparation of rGO-(U)BiOCl nanocomposites.
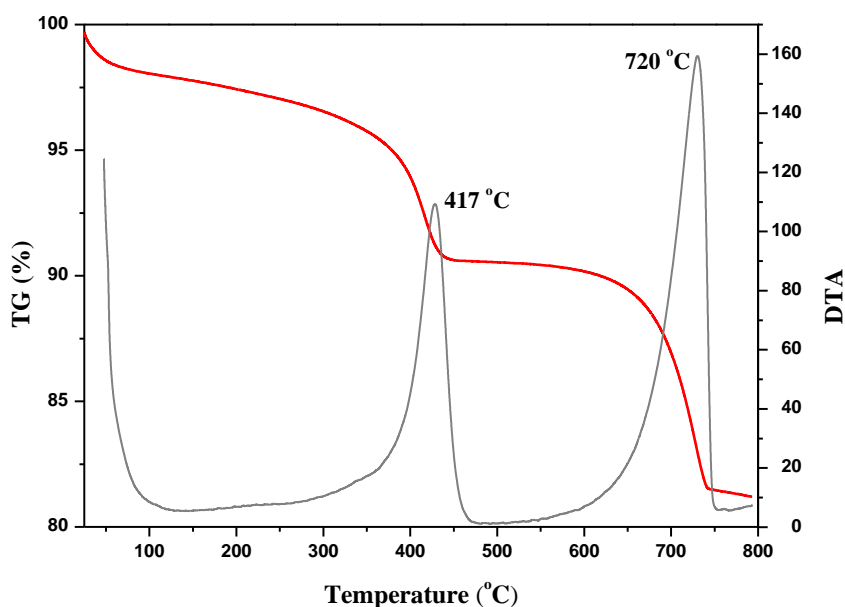

Figure 5. TG-DTA curves for rGO-(U)BiOCl.

To investigate the thermal stability of the rGO-(U)BiOCl, thermogravimetric analysis-differential thermal analysis (TG-DTA) was performed in air atmosphere with a heating rate of 10 °C min^{-1}. As temperature increased, the sample weight decreased (Figure 5). Before 100 °C, the samples exhibited significant weight reduction, which was attributed to the evaporation of water. At 417 °C, the samples showed 5% weight loss, which was attributed to the combustion of carbon layers [23]. When the temperature rose to 720 °C, another remarkable weight loss was observed because BiOCl was converted to Bi_2O_3 and $BiCl_3$ [24-26].
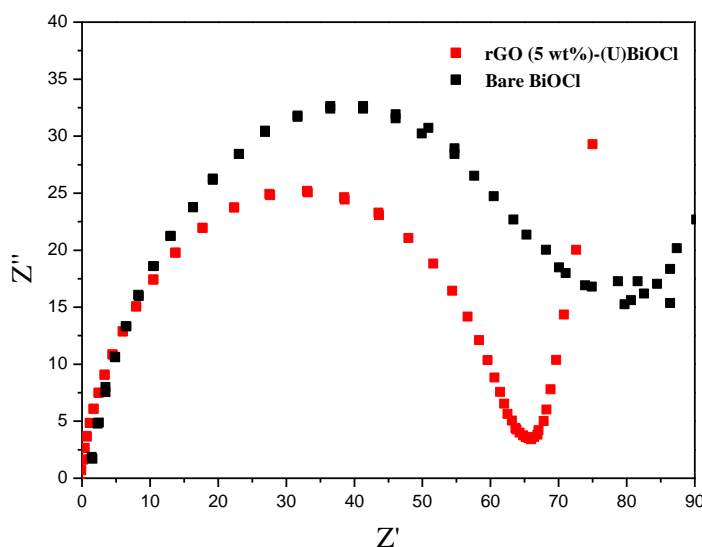
Figure 6. Nyquist plots of bare BiOCl and rGO(5 wt%)-(U)BiOCl.

Figure 6 illustrates the EIS results of bare BiOCl and rGO(5 wt%)-(U)BiOCl samples. Compared with bare BiOCl, the rGO(5 wt%)-(U)BiOCl sample show a smaller semicircle, indicating a lower charge-transfer resistance and faster interfacial charge-transfer process [13]. The rGO(5 wt%)-(U)BiOCl sample exhibits better electrochemical performance. Hence, it is remarkable that the rGO could notably enhance the electrochemical behavior of BiOCl.
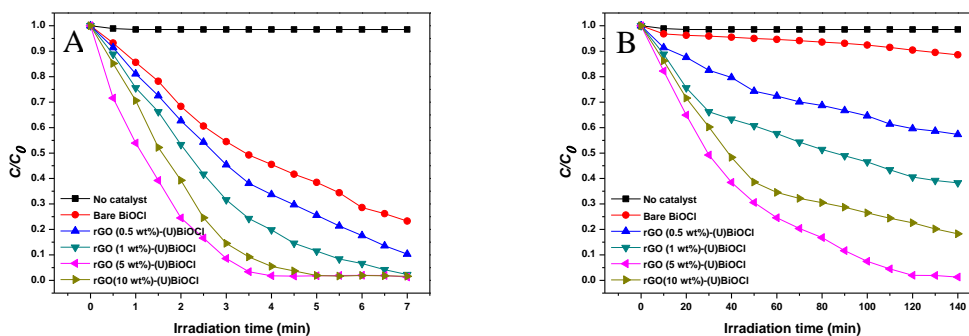
Figure 7. Photocatalytic degradation efficiency of bare BiOCl and rGO-BiOCl photocatalysts on RB with the irradiation of UV (A) or visible light (B).

The photocatalytic activities of BiOCl and rGO-(U)BiOCl were characterized by the degradation of RhB in an aqueous solution under UV and visible light irradiation. Figure 7 displays the change in absorption spectra of RhB aqueous solution under UV and visible light irradiation in the presence of BiOCl nanosheets and rGO-(U)BiOCl nanocomposites. Figure 7 shows that rGO could greatly improve the photocatalytic ability of BiOCl under both UV and visible light irradiation.

RhB was degraded faster after irradiation with UV than with visible light. Under UV, the degradation speed dramatically increased with the rGO content from 0.5 wt% to 5 wt% of rGO-

(U)BiOCl (see Figure 7(A)). In addition, rGO(5 wt%)-(U)BiOCl exhibited the best photocatalytic activity among the prepared rGO-(U)BiOCl nanocomposites. rGO(5 wt%)-(U)BiOCl could degrade 96% RhB within 3.5 min, whereas the bare BiOCl nanosheets could only degrade 50% at that time. Interestingly, excess rGO after 5 wt% of rGO-(U)BiOCl did not benefit the photocatalytic performance of rGO-(U)BiOCl. rGO(10 wt%)-(U)BiOCl exhibited lower photocatalytic activity than rGO(5 wt%)-(U)BiOCl. This result was probably because the excess rGO reduced the incident UV light on the BiOCl surface, thereby reducing the photocatalytic performance [27].

Figure 7(B) shows the photocatalytic effect of the bare BiOCl and rGO-BiOCl photocatalysts on the degradation of RhB under visible light, in which the experimental condition was identical to that under UV light. The bare BiOCl exhibited weak photocatalytic activity under visible light, and only 11.4% of RhB was degraded even after 140 h. By contrast, the rGO-BiOCl nanocomposites showed high photocatalytic property, because rGO plays an important role in the degradation of RhB on RGB hybrids under visible light.

4. CONCLUSIONS

A composite photocatalyst rGO-(U)BiOCl was successfully prepared through the controllable in situ growth of ultrathin BiOCl nanosheet solution on reduced GO. The optimal sample exhibited excellent photocatalytic activity in the degradation of RhB under UV and visible light irradiation. The rGO-(U)BiOCl composites showed better electrochemical behaviors and photocatalytic performances than bare BiOCl in the degradation of RhB dye under UV and visible light. The rGO-(U)BiOCl composites exhibit faster interfacial charge-transfer process, resulting a better electrochemical performance than bare BiOCl. The enhanced photocatalytic activity was attributed to the effective electron–hole separation and transportation, effective charge separation and transportation, and increased light absorption.

CONFLICTS OF INTEREST:
The authors declare no conflict of interest.

References

1. N. Liu, V. Haublein, X. M. Zhou, U. Venkatesan, M. Hartmann, M. Mackovic, T. Nakajima, E. Spiecker, A. Osvet, L. Frey and P. Schmuki, *Nano Lett.*, 15 (2015) 6815.
2. T. T. Zhang, Y. Luo, B. Jia, Y. Li, L. L. Yuan and J. Yu, *J. Environ. Sci-China*, 32 (2015) 108.

3.   M. Abdallah and M. E. Moustafa, *Annali di chimica*, 94 (2004) 601.
4.   W. K. Zhang and K. J. Gaffney, *Accounts Chem. Res.*, 48 (2015) 1140.
5.   O. Sheikhnejad-Bishe, A. Rajabtabar-Darvishi, E. Khodadad, A. Mostofizadeh, F. Zhao and Y. Huang, *Int. J. Electrochem. Sci.*, 9 (2014) 4230.
6.   T. D. Nguyen-Phan, S. Luo, Z. Y. Liu, A. D. Gamalski, J. Tao, W. Q. Xu, E. A. Stach, D. E. Polyansky, S. D. Senanayake, E. Fujita and J. A. Rodriguez, *Chem. Mater.*, 27 (2015) 6282.
7.   W. Sun, H. Chu, B. Dong, D. Cao and S. Zheng, *Int. J. Electrochem. Sci.*, 9 (2014) 4566.
8.   N. O. Weiss, H. L. Zhou, L. Liao, Y. Liu, S. Jiang, Y. Huang and X. F. Duan, *Adv. Mater.*, 24 (2012) 5782.
9.   P. H. Wobkenberg, G. Eda, D. S. Leem, J. C. de Mello, D. D. C. Bradley, M. Chhowalla and T. D. Anthopoulos, *Adv. Mater.*, 23 (2011) 1558.
10. C. E. Oh, Y. H. Park, S. Kim, D. Lim, S. Y. Park and I. In, *Chem. Lett.*, 44 (2015) 1068.
11. F. D. Gao, D. W. Zeng, Q. W. Huang, S. Q. Tian and C. S. Xie, *Phys. Chem. Chem. Phys.*, 14 (2012) 10572.
12. Z. C. Yang, F. X. Cheng, X. P. Dong and F. M. Cui, *Rsc Adv.*, **5** (2015) 68151.
13. Z. S. Liu, J. N. Niu, P. Z. Feng and Y. B. Zhu, *Ceram. Int.*, 41 (2015) 4608.
14. H. L. Poh, F. Sanek, A. Ambrosi, G. J. Zhao, Z. Sofer and M. Pumera, *Nanoscale*, 4 (2012) 3515.
15. T. Rath and P. P. Kundu, *Rsc Adv.*, 5 (2015) 26666.
16. J. S. Park and H. J. Choi, *Phys. Rev. B*, 92 (2015).
17. M. A. Velasco-Soto, S. A. Perez-Garcia, J. Alvarez-Quintana, Y. Cao, L. Nyborg and L. Licea-Jimenez, *Carbon*, 93 (2015) 967.
18. J. Tauc, R. Grigorovici and A. Vancu, *physica status solidi (b)*, 15 (1966) 627.
19. Q. J. Xiang, J. G. Yu and M. Jaroniec, *Chem. Soc. Rev.*, 41 (2012) 782.
20. X. Q. Xie, K. Kretschmer and G. X. Wang, *Nanoscale*, **7** (2015) 13278.
21. M. Sahoo, R. P. Antony, T. Mathews, S. Dash and A. K. Tyagi, *Solid State Physics,* 1512 (2013) 1262.
22. M. J. Allen, J. D. Fowler, V. C. Tung, Y. Yang, B. H. Weiller and R. B. Kaner, *Appl. Phys. Lett.*, 93 (2008).
23. F. Yavari, H. R. Fard, K. Pashayi, M. A. Rafiee, A. Zamiri, Z. Z. Yu, R. Ozisik, T. Borca-Tasciuc and N. Koratkar, *J. Phys. Chem. C*, 115 (2011) 8753.
24. H. Gnayem and Y. Sasson, *J. Phys. Chem. C*, 119 (2015) 19201.
25. M. A. Gondal, X. F. Chang, A. A. Al-Saadi, Z. H. Yamani, J. Zhang and G. B. Ji, *J. Environ. Sci. Heal. A*, 47 (2012) 1192.
26. S. J. Peng, L. L. Li, P. N. Zhu, Y. Z. Wu, M. Srinivasan, S. G. Mhaisalkar, S. Ramakrishna and Q. Y. Yan, *Chem-Asian J.*, 8 (2013) 258.
27. L. H. Tian, J. Y. Liu, C. Q. Gong, L. Q. Ye and L. Zan, *J. Nanopart. Res.*, 15 (2013).